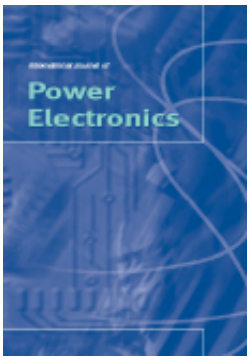

International Journal of Power Electronics

ISSN online: 1756-6398 - ISSN print: 1756-638X
https://www.inderscience.com/ijpelec

Phase locked loop parameterisation in AC/DC interconnected system for a multi-source AGC system under open market environment

Saha Debdeep, Saikia Lalit Chandra

DOI: 10.1504/IJPELEC.2023.10052288

Article History:

Received:	18 July 2020
Last revised:	19 January 2021
Accepted:	27 March 2021
Published online:	08 December 2022

Phase locked loop parameterisation in AC/DC interconnected system for a multi-source AGC system under open market environment

Saha Debdeep*

Department of Electrical Engineering,
Indian Institute of Engineering Science and Technology Shibpur,
West Bengal, India
Email: saha_debdeep_RS@yahoo.com
*Corresponding author

Saikia Lalit Chandra

Department of Electrical Engineering,
National Institute of Technology Silchar,
Assam, India
Email: lcsaikia@yahoo.com

Abstract: This article emphasises on deregulated AGC of a realistic multi-machine gas – thermal plant with dish-Stirling solar-thermal (DSTS) as additional power generation sources in each control area by taking into accounts of AC/DC with phase locked loop (PLL) dynamics. Eigenvalue analysis confirms the steadiness of the reasonable power system with various interconnections such as AC, AC/DC link and AC/DC with PLL dynamics. A series form of proportional-integral-derivative (PID) namely proportional gain cascaded with integral and double-derivative (PI^+DD^+) controller is employed as secondary controller in each control areas for robust AGC to carry out market transactions under deregulated environment. Exploring the system with different type of interconnections infer that proper tuning of PLL function parameters may synchronise the grid better than without employing PLL. The performance of PI^+DD^+ controller along with optimum PLL gains commensurate with wide variations in governor, turbine, fuel and compressor discharge time constant of gas turbine plant.

Keywords: automatic generation control; dish-Stirling solar thermal; deregulated; eigenvalue; phase locked loop; PLL; series controller.

Reference to this paper should be made as follows: Debdeep, S. and Chandra, S.L. (2023) 'Phase locked loop parameterisation in AC/DC interconnected system for a multi-source AGC system under open market environment', *Int. J. Power Electronics*, Vol. 17, No. 1, pp.1–28.

Biographical notes: Saha Debdeep received his BE in 2010 in Electrical Engineering from the Dibrugarh University and ME in 2014 in Power Systems from the Gauhati University, Assam, India. He is awarded the PhD in Power and Energy System at the National Institute of Technology Silchar, India in 2019. His research interests are automatic generation control, soft computing applications in power system operation, etc. He is presently working in the Department of Electrical Engineering, Indian Institute of Engineering Science and Technology Shibpur.

Saikia Lalit Chandra graduated in Electrical Engineering from the Dibrugarh University, Assam, in 1993. He joined in North Eastern Drilling and Work over Services, Company (PVT) Ltd., Digboi, Assam in December 1992 as an electrical engineer. In December 1993, he joined as a rig electrical engineer in ONGCL RECAPICOL, Sibsagar, Assam and worked till 1997. He started his teaching life as a Part-time Lecturer in the Jorhat Engineering College, Jorhat, Assam in 1997. In 2000, he joined as a Lecturer in the Electrical Engineering Department, NIT Silchar and also received his MTech in Power Systems from the Indian Institute of Technology, Delhi in 2007. He has achieved his PhD in Electrical Engineering in April 2012 from the National Institute of Technology, Silchar, Assam. Presently he is working as an Associate Professor in the Department of Electrical Engineering, NIT Silchar.

1 Introduction

Deregulated power system has facilitated large amount of power exchanges among the control areas for long distances which in turn has introduced power electronic apparatus in power grid (Bevrani and Hiyama, 2014). Rapid growth of multi-area interconnected system has transformed the power network into a complex one and made a challenging task for frequency control in AC/DC system (Kumar and Kothari, 2005). DC systems are competent enough for transferring power over longer distances and thereby interconnecting networks with different frequencies which results in higher interests amongst industry and academia (Elgerd and Fosha, 1970; Kundur, 1994).

The assessment of AGC in an open market environment is provided in detail in Donde et al. (2001) and Bjorn and Ove (1998). It also states information over deregulation and evaluates the AGC simulation during Pool Co., bilateral and contract violation cases after deregulation. Among the conventional sources of generation such as thermal (Debbarma et al., 2014), thermal-thermal (Guha et al., 2017), hydrothermal (Bjorn and Ove, 1998; Rao et al., 2009), wind-diesel (Rao and Das, 2015), gas-thermal (Hota and Banaja, 2016), hydro-thermal-gas (Mahendra et al., 2017), gas turbines share unique frequency response features in comparison to others. The power output does not completely depend on the governor during uncertain frequency fluctuations. A sole and two – area realistic hydro-thermal-gas system under conventional environment is studied by Arya (2017). Arya and Kumar (2017) also investigated a two area hydro – thermal and a two area gas – thermal system under deregulated environment. During frequent change in frequency in electricity networks, there is an impact on gas turbines which influence system stability (Lasantha, 2014). Frequency regulation of AC/DC incorporated interconnected multi-source hydrothermal power system under open market scenario to simulate the three transaction scenarios such as Pool Co., bilateral and contract violation (Arya and Kumar, 2016). Sharma et al. (2016) presented the design of AGC controllers for a multi-area AC/DC power system having diverse type turbines. Ibraheem and Bhatti (2014) and Singh et al. (2014) and presented a comprehensive study on parallel AC/DC incorporated dynamic performance of system with many sources comprising of thermal, hydro and gas in each area. To avoid HVAC limitations for improving the LFC performance, a new additional controller for a bi-directional VSC-HVDC system is proposed (Zhou et al., 2014). Zhou et al. (2014) studied the phase locked loop (PLL) factors on the behaviour of a voltage-source converter (VSC) integrated HVDC

transmission power system. The synchronism of VSC-HVDC converter along with the AC/DC transmission link is done by PLL model. Rakhshani et al. (2016, 2012) analysed the active effects of HVDC links allowing for second-order PLL function during coordination with AC system. Saha and Saikia (2017a) modelled a conventional environment integrated with PLL in a CCGT incorporated system employed with AC/DC interconnection under conventional environment. However, it is rare (Rakhshani et al., 2014) to find a literature with multi-area gas-thermal system employing AC/DC interconnection under deregulated environment and where PLL dynamics is demonstrated.

The declining of fossil fuel and the ill effects of conventional sources to environment has increased the importance of power system studies including renewable energy source in power system studies. Recent technologies on solar energy are available in recent literatures (Rahman et al., 2016, 2017; Das et al., 2014), but only the stand-alone systems are studied (Rao and Das, 2015). Rahman et al. (2016, 2017) emphasised on dish-Stirling solar thermal system (DSTS) in solving AGC problem. Rao and Das (2015) describes a system comprising a wind turbine generator and a diesel generator. Das et al. (2014) demonstrated an isolated hybrid system with dish-Stirling solar thermal systems (DSTS) in integration with diesel engine generators, fuel cells, battery energy storage system, and aqua electrolyser. So, far it is difficult to find any literature which studies the effect of PLL in a renewable energy sources penetrated gas – thermal plant. Moreover these authors except few (Rahman et al., 2016, 2017) have neglected nonlinearity like generation rate constraint (GRC) and governor dead band (GDB) together and hence their work has a limitation on working of AGC in deregulated environment with consideration of nonlinearities. Moreover, very little literature (Arya and Kumar, 2016; Sharma et al., 2016; Ibraheem and Bhatti, 2014) comment on stability of the test system considered with different interconnections.

A sustained oscillation develops in the plant due to the presence of nonlinearities such as GDB and GRC in the system. The counter attack to this phenomenon can be treated with a supplementary controller of robust nature. Various literatures has utilised optimal AGC regulators (Elgerd and Fosha, 1970; Arya and Kumar, 2016; Sharma et al., 2016), classical controllers such as PI, proportional-integral-derivative (PID) (Hota and Banaja, 2016; Rahman et al., 2017; Das et al., 2014), three degree of freedom PID (Rahman et al., 2016), fuzzy PI (Rao and Das, 2015) to simulate all possible market transactions in a deregulated scenario (Elgerd and Fosha, 1970; Arya and Kumar, 2016; Sharma et al., 2016) and successfully mitigated frequency and tie-power deviations in interconnected system. A series form of PID controller (Johnson and Moradi, 2000) exists which offers the same benefits as of parallel PID controller. Few industries retain the series form to maintain the analogue circuitry in industries. Ideal series PID controller has been applied to obtain a high performance/robustness trade-off in nonlinear systems (Johnson and Moradi, 2000; Miroslav et al., 2014). However, no such literature provides and information of performance of series PID controller in hybrid gas-thermal system employed with AC/DC interconnection. A new form of series PID controller namely proportional gain cascaded with integral and double-derivative ($PI^{+}DD^{+}$) has been introduced in the present work as a secondary controller to minimise the area control error. Use of extra derivative will help in diminishing the oscillations due to presence of DSTS, GRC and GDB. The gains and other parameters of secondary controller need to be optimised using several optimisation techniques for healthier AGC system. The optimisation algorithms such as genetic algorithm (Hota and Banaja, 2016), differential

evolution (Hota and Banaja, 2016), firefly algorithm (FA) (Debbarma et al., 2014) teaching-learning-based optimisation (Guha et al., 2017), quasi oppositional harmony search algorithm (QOHSA) (Mahendra et al., 2017), and biogeography-based optimisation (BBO) (Rahman et al., 2016, 2017), have been successfully applied in AGC problems for simultaneous optimisation of controller parameters and other system parameters. A metaheuristic algorithm inspired by the natural phenomenon of growth, known as stochastic fractal search (SFS) was presented by Hamid in 2015. It uses a mathematical concept of fractals where random fractals spread the unit. The global optimum result is achieved in a minimum number of iterations and thus improves accuracy (Iasef and Shuichi, 2016; Mellal and Zio, 2016; Saha and Saikia, 2017b; Sabir and Ibrir, 2019). So far, it is rare (Hamid, 2015) to find any literature that deals with the concept of random fractals for optimisation of $PI^{+}DD^{+}$ gains engaged in diverse sources deregulated system incorporating PLL dynamics. In observation to the above, objectives of the article are framed as follows:

1 To design a two control area interconnected gas-thermal system incorporating DSTS plant under deregulated environment with consideration of realistic constraints. Three types of interconnections are considered namely AC tie, AC/DC tie and, AC/DC tie line interconnection with PLL dynamics and delay effects.

2 To investigate the dynamic stability by open loop eigenvalues with consideration of three interconnections namely AC, AC/DC and, AC/DC interconnection and PLL dynamics.

3 To compare the system dynamic responses with parallel and proposed form of series PID controller considering Pool Co. transactions and AC interconnection only and to determine the best controller suited.

4 To synchronise the grid with selection of optimal gains and parameters of PLL dynamics under bilateral transactions and contract violation scenario. To evaluate the robustness of optimal PLL parameters under violations in contracted load demand condition.

5 To demonstrate the performance of best controller obtained in 3 along with PLL dynamics for varied system conditions such as change in time constants of thermal and gas plant.

2 Power system investigated

The test model is a two-area AC interconnected power system consisting of reheat thermal and gas power plants in two GENCOs – gas and thermal in each control area (Arya and Kumar, 2016). Dish Stirling Solar Thermal Plant is integrated in each control area as additional sources to maintain the additional generation due to load changes. Each control area owns two DISCOs. A schematic diagram representing the mentioned scenario is provided in Figure 1(a). The capacity of area 2 is half of the first area. The system data can be obtained from Hota and Banaja (2016) and Mahendra et al. (2017) and are noted in Appendix 1. To attain realistic outcome, appropriate GRC models of 3%/min for the reheat thermal and 20%/min for the gas plants and, transfer function modelling of appropriate GDB of the reheat thermal plants are taken into account (Elgerd

and Fosha, 1970; Hota and Banaja, 2016). The transfer function model of the AC interconnected gas thermal system with DSTS as additional generation under deregulated environment is shown in Figure 1(b). Open communication channels of 20 ms are provided in each control area. ITAE is considered as the performance index to minimise the area control error, i.e., minimising the peak deviations and settling time, which is given by equation (1).

$$J_{ITAE} = \int_0^T \left\{ \left|\Delta F_i\right| + \left|\Delta P_{tiei-j}\right| \right\} t \cdot dt \tag{1}$$

DSTS unit in both areas are not considered in the contracted transactions, although it maintains the adequate generation in the control area due to the load change. This article considers only the low frequency sphere and hence the simplified first order transfer function a DSTS plant is referred from Das et al. (2014). However, the approximate power output equation of Stirling engine has been referred from Das et al. (2014).

$$P_{eng} = 0.015 P_{mean} V_{disp} f \tag{2}$$

where f is the frequency in Hz, P is the power output of engine in watts, P_{mean} is the mean cycle pressure in bar, V_{disp} is the power piston displaced in cm^3. DPM defines the area participation factor of each GENCO in each control area. In Pool Co. type, GENCOs of one area provide the load demanded by the same area DISCOs. In bilateral type, DISCOS of any area can contract with GENCOs of any area. In an open market scenario, bilateral and Pool Co. transaction can occur simultaneously.

$$\Delta P_{tie12}^{scheduled} = \sum_{i=1}^{2}\sum_{j=3}^{4} cpf_{ij}\Delta P_{Lj} - \sum_{i=3}^{4}\sum_{j=1}^{2} cpf_{ij}\Delta P_{Lj} \tag{3}$$

$$\Delta P_{tie12}^{error} = \Delta P_{tie12}^{actual} - \Delta P_{tie12}^{scheduled} \tag{4}$$

Figure 1 First order modelling of considered test system, SPMC and proposed controller,
(a) schematic diagram of gas-thermal system with DSTS as additional source
(b) transfer function modelling of gas-thermal system under deregulated environment
(see online version for colours)

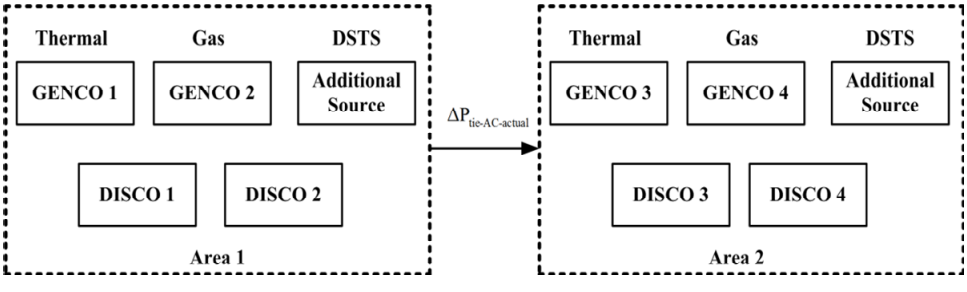

(a)

Figure 1 First order modelling of considered test system, SPMC and proposed controller, (a) schematic diagram of gas-thermal system with DSTS as additional source (b) transfer function modelling of gas-thermal system under deregulated environment (continued) (see online version for colours)

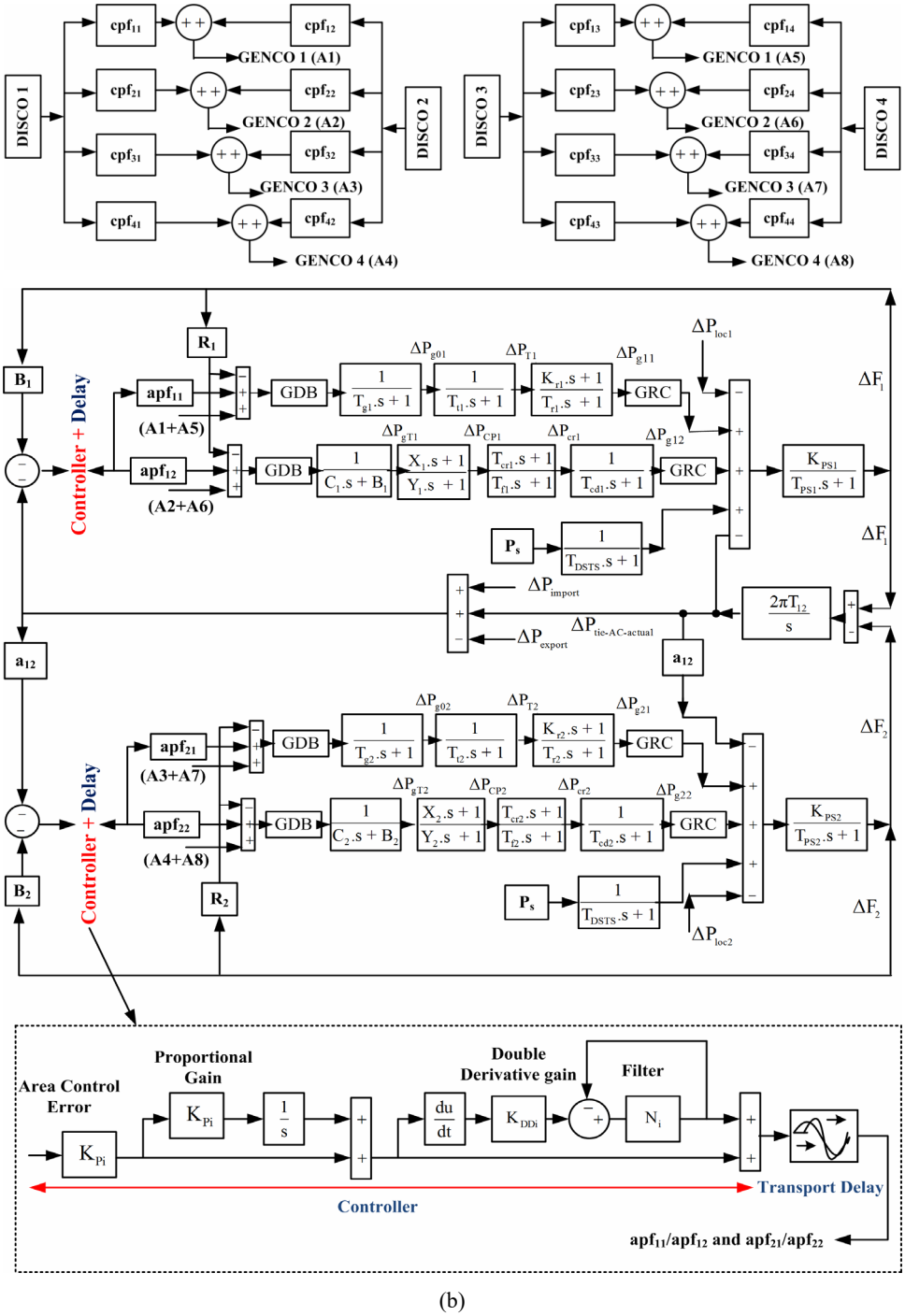

(b)

3 PLL dynamics

A device which generates one signal to track another signal is known as PLL. The reference signal and the output signal are synchronised in phase as well as in frequency. A phase detector (PD), a loop filters (LFs), and a voltage-controlled oscillator (VCO) (Rakhshani et al., 2016) constitutes a PLL. The difference of any two input signals which is oscillating can be contained by PD and is non linear in nature. PD limits the tracking range and lock limit. VCO provides stability in phase, frequency deviation, control voltage, and capability for accepting wide-band modulation. It suppresses the noise signal and high-frequency signal from the PD and initiates a dc-controlled signal for the VCO. The phase error voltage is filtered by the loop LF. Presence of an integrator makes it a type two LFs.

Figure 2 Transfer function model of AC/DC with PLL dynamics interconnected gas-thermal system with DSTS as additional sources under deregulated environment (see online version for colours)

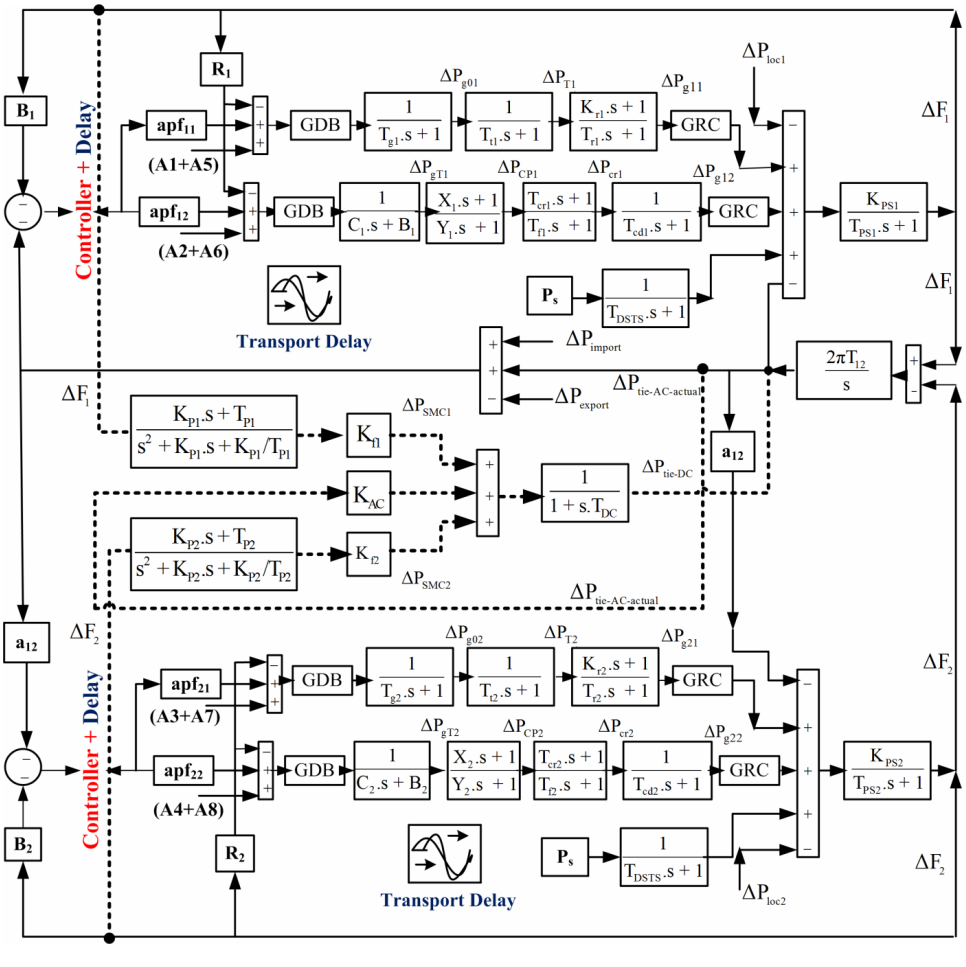

A high-gain active filter second-order PLL can be approximated as a type – two loop, whereas a passive filter PLL is type one (Rakhshani et al., 2016). PLL has a purpose of providing the angle of grid voltage. This PLL estimates the frequency. Referring to the small signal model of PLL (Rakhshani et al., 2012), the open loop and closed loop transfer function considering ($K_{PD} = K_{VCO} = 1$) can be given by equations (5) and (6).

$$P_{OL}(s) = PD(s) \cdot LF(s) \cdot VCO(s) = \frac{\left(K_{pi}s + \frac{K_{pi}}{T_i}\right)}{s^2} \tag{5}$$

$$Q_{CL}(s) = \frac{P_{OL}(s)}{1 + P_{OL}(s)} = \frac{\left(K_{pi}s + \frac{K_{pi}}{T_i}\right)}{\left(s^2 + K_{pi}s + \frac{K_{pi}}{T_i}\right)} \tag{6}$$

It is clear that equation (6) refers to type-2 system, which has two poles at the origin. The low pass filter in PLL [equation (6)] detects the input voltage angle and attenuates the detection error caused by noise and higher order harmonics in the input signal (Saha and Saikia, 2017a).

Normalising the PLL transfer function in second order as follows:

$$Q_{CL_{PLL}}(s) = \frac{2\zeta\omega_n + \omega_n^2}{s^2 + 2\zeta\omega_n + \omega_n^2} \tag{7}$$

where natural frequency, $\omega_n = \sqrt{\frac{K_{pi}}{T_i}}$ and Damping coefficient, $\zeta = \sqrt{\frac{K_{pi}T_i}{2}}$.

For 1% steady state response, approximated time constant can be $\lambda = \frac{1}{\zeta_i \omega_{ni}}$. The modelling of HVDC link for implementation of PLL dynamics as damping controller to damp out the load changes leads to design of a supplementary power modulation controller (SPMC) (Rakhshani et al., 2016). The transfer function model in Figure 1(b) is not interconnected with AC/DC and PLL dynamics and is presented as Figure 2. The dotted lines in Figure 2 presents the SPMC to incorporated the second order PLL dynamics. When there is a frequency variation at two sides of the DC link, modulation of power flow is done by the VSC-HVDC link. Here, fast transients of HVDC parts are neglected as the electronic parts offer less time constant than mechanical part in power system. The control signal for the converter is the frequency deviation which controls the power flow with converter duty cycle change. The equation governing the HVDC link can be written as follows:

$$\Delta X_{DC} = K_{f1}\Delta F_1(PLL) + K_{ac}\Delta P_{tie-AC-actual} + K_{f2}\Delta F_2(PLL) \tag{8}$$

ΔX_{DC} is the input signal of AC/DC line developed due to deviation in frequency and tie-power (Wang et al., 2019). The transfer function of HVDC link is given by a first order function as in:

$$\Delta P_{DC} = \frac{1}{1 + sT_{DC}}\Delta F \tag{9}$$

For utilising the AC/DC interconnection without PLL dynamics, the gains K_{f1}, K_{f2} and K_{AC} along with the second order function [equation (6)] should be excluded in the model.

4 Design of proportional gain cascaded with integral and double-derivative (PI^+DD^+) controller

Parallel PID controllers have always been popular in control and engineering platform due to easy realisation, utilisation, cheap and simplicity. To maintain the efficient continuity in later PID devices, which used pneumatic systems, the structure in series is retained (Johnson and Moradi, 2000). Recent classical PID controllers are in parallel numerical form, but the industrial manuals still contain these series PID controller (Johnson and Moradi, 2000; Miroslav et al., 2014) due to its reliable usage so far. This article proposes a series form of PID controller with an additional derivative term to it known as series proportional gain cascaded with integral and double derivative gain (PI^+DD^+) controller as in Figure 3.

Figure 3 First order model of series proportional gain cascaded with integral and double derivative gain (PI^+DD^+) controller

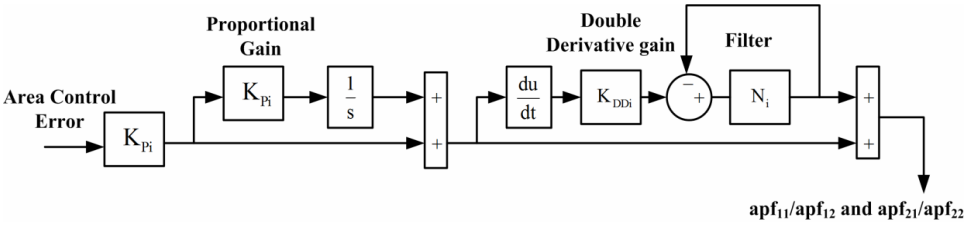

The transfer function of a series PID controller is given by equation (10).

$$U_{se}(s) = \left[K_s \left(1 + \frac{1}{sT_i} \right) (1 + sT_d) \right] E(s) \tag{10}$$

The transfer function of the proposed PI^+DD^+ controller is given by equation (11).

$$U_{se}(s) = \left[K_s \left(1 + \frac{1}{sT_i} \right) \left(1 + T_d \frac{s^2 N}{(N + s)} \right) \right] E(s) \tag{11}$$

Under disturbed or noisy situation, additional derivative term will influence the disturbances and hence a first order filter is introduced to curtail the unwanted effect of the high-frequency amount noise.

The controller parameters and other system parameters are optimised by SFS algorithm (Hamid, 2015) considering the performance index is given in equation (1). Various literature (Hamid, 2015; Iasef and Shuichi, 2016; Mellal and Zio, 2016) has utilised the fractal property of growth in solving engineering applications such as reliability assessment (Mellal and Zio, 2016), architecture and construction (Iasef and Shuichi, 2016), load frequency control (Saha and Saikia, 2017a), etc. It comprises of diffusion and two-staged updating process. SFS algorithm exchange information among the participants in a group which in turn accelerate convergence and accuracy as it helps

in determining the global minima. The description, flowchart and pseudo code is depicted beautifully in Hamid (2015) and Iasef and Shuichi (2016). The optimum factors of the SFS algorithm are considered as population size = 70, maximum generation = 60, maximum diffusion number (MDN) = 2 and diffusion walk = 0.75. 50 trial runs are considered with minimisation of the cost function. In each trial (not shown), the minimum tuned factor (increased in steps) is selected as optimum keeping the other factor fixed. Similarly, all the tuned parameters are obtained till the minimum cost function value is attained. Thus, the limits of controller gains and filter-coefficient range from 0 to 1 and 1 to 100 respectively.

5 Eigenvalue analysis for the two area gas-thermal deregulated system

It is necessary to determine eigenvalue for understanding the stability of the deregulated system when interconnected with AC tie, AC/DC tie and AC/DC tie integrating PLL dynamics. DSTS plant as an additional source is not considered in the process for analysis. Referring to Figure 1(b), 19 state variables are identified for the system with AC interconnection; 5 more variables are included for AC/DC interconnection with PLL dynamics (Figure 2). The nomenclature of state variables is noted in Appendix 2. Introduction of the system parameters are the standard parameters considered from Elgerd and Fosha (1970) and are provided in nomenclature. Firstly, state space considering AC interconnection only:

$$\dot{\Delta F_1}(s) = -\frac{1}{T_{PS1}}\Delta F_1(s) + \frac{K_{PS1}}{T_{PS1}}\Delta P_{g11}(s) + \frac{K_{PS1}}{T_{PS1}}\Delta P_{g12}(s) - \frac{K_{PS1}}{T_{PS1}}\Delta P_{tie12}(s) \tag{12}$$

$$\dot{\Delta P_{g11}}(s) = \frac{K_{r1}}{T_{r1}T_{t1}}\Delta P_{g01}(s) - \frac{1}{T_{r1}}\Delta P_{g11}(s) + \frac{(T_{t1} - K_{r1})}{T_{r1}T_{t1}}\Delta P_{T1}(s) \tag{13}$$

$$\dot{\Delta P_{T1}}(s) = \frac{1}{T_{t1}}\Delta P_{g01}(s) - \frac{1}{T_{t1}}\Delta P_{t1}(s) \tag{14}$$

$$\dot{\Delta P_{g01}}(s) = \frac{apf_{11}}{T_{g1}}\Delta P_{C1}(s) - \frac{1}{T_{g1}R_1}\Delta F_1(s) - \frac{1}{T_{g1}}\Delta P_{g01}(s) + \frac{(cpf_{11} + cpf_{21} + cpf_{31} + cpf_{41})}{T_{g1}} \tag{15}$$

$$\dot{\Delta P_{gT1}}(s) = \frac{apf_{12}}{c_1}\Delta P_{C1}(s) - \frac{1}{c_1R_1}\Delta F_1(s) - \frac{b_1}{c_1}\Delta P_{T1}(s) + \frac{(cpf_{12} + cpf_{22} + cpf_{32} + cpf_{42})}{c_1} \tag{16}$$

$$\frac{X_1(cpf_{12} + cpf_{22} + cpf_{32} + cpf_{42})}{Y_1c_1} \tag{17}$$

$$\begin{aligned}\dot{\Delta P_{cr1}}(s) &= -\frac{T_{cr1}}{Y_1 T_{f1}}\Delta P_{CP1}(s)+\left(\frac{T_{cr1}}{T_{f1}Y_1}-\frac{b_1 X_1 T_{cr1}}{T_{f1}Y_1 c_1}\right)\Delta P_{gT1}(s)\\ &-\frac{X_1 T_{cr1}}{T_{f1}c_1 R_1 Y_1}\Delta F_1(s)+\frac{apf_{12}X_1 T_{cr1}}{T_{f1}Y_1 c_1}\Delta P_{c1}(s)\\ &+\frac{X_1 T_{cr1}\left(cpf_{12}+cpf_{22}+cpf_{32}+cpf_{42}\right)}{Y_1 c_1}\\ &-\frac{1}{T_{f1}}\Delta P_{cr1}(s)+\frac{1}{T_{f1}}\Delta P_{CP1}(s)\end{aligned} \tag{18}$$

$$\dot{\Delta P_{g12}}(s) = \frac{1}{T_{cd1}}\Delta P_{cr1}(s)-\frac{1}{T_{cd1}}\Delta P_{g12}(s) \tag{19}$$

$$\dot{\Delta P_{tie12}}(s) = 6.28T_{12}\left(\Delta F_1(s)-\Delta F_2(s)\right) \tag{20}$$

$$\dot{\Delta F_2}(s) = -\frac{1}{T_{PS2}}\Delta F_2(s)+\frac{K_{PS2}}{T_{PS2}}\Delta P_{g21}(s)+\frac{K_{PS1}}{T_{PS1}}\Delta P_{g22}(s)-\frac{a_{12}K_{PS2}}{T_{PS2}}\Delta P_{tie12}(s) \tag{21}$$

$$\dot{\Delta P_{g21}}(s) = \frac{K_{r2}}{T_{r2}T_{t2}}\Delta P_{g02}(s)-\frac{1}{T_{r2}}\Delta P_{g21}(s)+\frac{\left(T_{t2}-K_{r2}\right)}{T_{r2}T_{t2}}\Delta P_{T2}(s) \tag{22}$$

$$\dot{\Delta P_{T2}}(s) = \frac{1}{T_{t2}}\Delta P_{g02}(s)-\frac{1}{T_{t2}}\Delta P_{t2}(s) \tag{23}$$

$$\begin{aligned}\dot{\Delta P_{g02}}(s) &= \frac{apf_{21}}{T_{g2}}\Delta P_{C2}(s)-\frac{1}{T_{g2}R_2}\Delta F_2(s)-\frac{1}{T_{g2}}\Delta P_{g02}\\ &+\frac{\left(cpf_{13}+cpf_{23}+cpf_{33}+cpf_{43}\right)}{T_{g1}}(s)\end{aligned} \tag{24}$$

$$\begin{aligned}\dot{\Delta P_{gT2}}(s) &= \frac{apf_{22}}{c_2}\Delta P_{C2}(s)-\frac{1}{c_2 R_2}\Delta F_2(s)-\frac{b_2}{c_2}\Delta P_{T2}(s)\\ &+\frac{\left(cpf_{14}+cpf_{24}+cpf_{34}+cpf_{44}\right)}{c_2}\end{aligned} \tag{25}$$

$$\begin{aligned}\dot{\Delta P_{CP2}}(s) &= -\frac{1}{Y_1}\Delta P_{CP2}(s)+\left(\frac{1}{Y_2}-\frac{b_2 X_2}{T_{f2}Y_2 c_2}\right)\Delta P_{gT2}(s)\\ &-\frac{X_2}{c_2 R_2 Y_2}\Delta F_2(s)+\frac{apf_{22}X_2}{Y_2 c_2}\Delta P_{c2}(s)\\ &+\frac{X_2\left(cpf_{14}+cpf_{24}+cpf_{34}+cpf_{44}\right)}{Y_2 c_2}\end{aligned} \tag{26}$$

$$\dot{\Delta P_{cr2}}(s) = -\frac{T_{cr2}}{Y_2 T_{f2}}\Delta P_{CP2}(s)+\left(\frac{T_{cr2}}{T_{f2}Y_2}-\frac{b_2 X_2 T_{cr2}}{T_{f2}Y_2 c_2}\right) \tag{27}$$

$$\Delta P_{gT2}(s)-\frac{X_2T_{cr2}}{T_{f2}c_2R_2Y_2}\Delta F_2(s)+\frac{apf_{22}X_2T_{cr2}}{T_{f2}Y_2c_2}\Delta P_{c2}(s)$$
$$+\frac{X_2T_{cr2}\left(cpf_{14}+cpf_{24}+cpf_{34}+cpf_{44}\right)}{Y_1c_1}-\frac{1}{T_{f2}}\Delta P_{cr2}(s)+\frac{1}{T_{f2}}\Delta P_{CP2}(s) \quad (28)$$

$$\dot{\Delta P}_{g22}(s)=\frac{1}{T_{cd2}}\Delta P_{cr2}(s)-\frac{1}{T_{cd2}}\Delta P_{g22}(s) \quad (29)$$

Addition of DC link in both areas along with AC interconnection urges the changes in two state variables (Frequency deviation and DC power deviation) given by equations (30)–(33). However, the other equation remains the same.

$$\dot{\Delta F_1}(s)=-\frac{1}{T_{PS1}}\Delta F_1(s)+\frac{K_{PS1}}{T_{PS1}}\Delta P_{g11}(s)+\frac{K_{PS1}}{T_{PS1}}\Delta P_{g12}(s)$$
$$-\frac{K_{PS1}}{T_{PS1}}\Delta P_{tie12}(s)-\frac{K_{PS1}}{T_{PS1}}\Delta P_{DC1}(s) \quad (30)$$

$$\dot{\Delta F_2}(s)=-\frac{1}{T_{PS2}}\Delta F_2(s)+\frac{K_{PS2}}{T_{PS2}}\Delta P_{g22}(s)+\frac{K_{PS2}}{T_{PS2}}\Delta P_{g22}(s)$$
$$-\frac{a_{12}K_{PS2}}{T_{PS2}}\Delta P_{tie12}(s)-\frac{K_{PS2}}{T_{PS2}}\Delta P_{DC2}(s) \quad (31)$$

$$\dot{\Delta P}_{DC1}=-\frac{1}{T_{DC1}}\Delta F_1(s)+\frac{1}{T_{DC1}}\Delta P_{DC1} \quad (32)$$

$$\dot{\Delta P}_{DC2}=-\frac{1}{T_{DC2}}\Delta F_2(s)+\frac{1}{T_{DC2}}\Delta P_{DC2} \quad (33)$$

Now, with consideration of PLL dynamics, two variables are added namely SPMC power deviation in both areas. Thus, DC power deviation, SPMC power deviations are given by equations (34)–(36).

$$\dot{\Delta P}_{SMC1}=\frac{0.35}{T_{PS1}}\Delta F_1(s)+\frac{0.35K_{PS1}}{T_{PS1}}\Delta P_{g11}(s)$$
$$+\frac{0.35K_{PS1}}{T_{PS1}}\Delta P_{g12}(s)-\frac{0.35K_{PS1}}{T_{PS1}}\Delta P_{g12}(s)\frac{0.35K_{PS1}}{T_{PS1}}\Delta P_{tie12}(s)$$
$$+0.4\Delta F_1(s)-0.095\Delta P^{I}_{SMC1}-0.095\Delta P_{SPMC1} \quad (34)$$

$$\dot{\Delta P}_{SMC2}=\frac{0.35}{T_{PS2}}\Delta F_2(s)+\frac{0.35K_{PS2}}{T_{PS2}}\Delta P_{g21}(s)++\frac{0.35K_{PS2}}{T_{PS2}}\Delta P_{g12}(s)$$
$$-\frac{0.35K_{PS1}}{T_{PS1}}\Delta P_{tie12}(s)+0.4\Delta F_1(s)-0.095\Delta P^{I}_{SMC2}-0.095\Delta P_{SPMC2} \quad (35)$$

$$\dot{\Delta P}_{DC}=-\frac{1}{T_{DC}}\Delta P_{DC}+\frac{1}{T_{DC}}\left[\dot{\Delta P}_{SMC1}+K_{ac}\Delta P_{tie12}+\dot{\Delta P}_{SMC2}\right] \quad (36)$$

For AC/DC and AC/DC interconnection with PLL, the values of time constant, gains and other parameters are referred from Singh et al. (2014). Using equations (12)–(36), open loop eigenvalues are determined for each interconnection and are tabulated as Table 1 for fair comparison.

Table 1 Open loop eigenvalues for the gas–thermal system with the three interconnected systems: AC link, AC/DC tie line and, AC/DC tie line integrated with PLL

State variable		*Eigenvalues with*		
		AC links	*AC/DC links*	*AC/DC and PLL*
1	ΔF_1	–12.934	–12.576	–12.609 + 0.000i
2	ΔP_{g11}	–12.534	–12.508	–12.508 + 0.000i
3	ΔP_{T1}	–3.2520 + 2.780i	–4.6317 + 6.370i	–0.9750 + 4.986i
4	ΔP_{g01}	–3.2520 – 2.789i	–4.6317 – 6.370i	–0.9750 – 4.986i
5	ΔP_{gT1}	–5.7484	–5.0112 + 5.970i	–4.9365 + 5.950i
6	ΔP_{CP1}	–5.4600	–5.0112 – 5.970i	–4.9365 – 5.950i
7	ΔP_{cr1}	–4.1743	–0.7064	–5.5086 + 5.383i
8	ΔP_{g12}	–2.4761 + 1.285i	–0.5399	–5.5086 – 5.383i
9	ΔP_{tie12}	–2.4761 – 1.285i	–0.2182 + 0.341i	–0.5622 + 0.000i
10	ΔF_2	–3.4757	–0.2182 – 0.341i	–0.1714 + 0.396i
11	ΔP_{g21}	–0.2994 + 1.474i	–0.1506	–0.1714 – 0.396i
12	ΔP_{T2}	–0.2994 – 1.47i	–0.9769	–0.2196
13	ΔP_{g02}	–1.4745	–1.0152	–0.9655
14	ΔP_{gT2}	–0.6171	–1.8689	–1.0123
15	ΔP_{CP2}	–0.1972 + 0.310i	–2.8298	–2.1719
16	ΔP_{cr2}	–0.1972 – 0.310i	–5.3042	–2.8622
17	ΔP_{g22}	–0.0928	–3.9512	–5.3634
18	ΔP_{C1}	–0.0304	–5.0131	–3.9326
19	ΔP_{C2}	–0.0000	–4.9940	–5.0781
20	ΔP_{DC1}	------	–4.3345	------
21	ΔP_{DC2}	------	–4.3412	------
22	ΔP_{SMC1}	------	------	–4.9941
23	ΔP_{SMC2}	------	------	–4.3472
24	ΔP_{DC}	------	------	–4.3349

From Table 1, it can be inferred that: firstly all negative values confirm the stability in three cases and secondly, relative stability is more in case of DC interconnection as the roots are located much far from the origin.

6 Simulations and discussion of results

A detailed analysis is of utmost necessity to evaluate the effects of different interconnection along with PLL dynamics in AGC of a two-area deregulated system. The three open market cases namely Pool Co., Bilateral transactions and contract violation are

investigated for the test system performance. The test system are implemented on MATLAB^{R} to discover the dynamic responses for ΔF_i, $\Delta P_{tie(i-j)}$, ΔP_{Ci} and ΔP_{gi} for 50% loading in both areas.

6.1 Scenario 1: comparison of parallel PID and proposed PI^{+}DD^{+} controller (Pool Co. transactions)

We consider that GENCOs in area 1 exhibit equal participation in AGC. The DPM is shown in equation (37), as presented by Donde et al. (2001). A 0.03 p.u. step load change is assumed to occur at area 1.

$$DPM_{PC} = \begin{bmatrix} 0.5 & 0.5 & 0 & 0 \\ 0.5 & 0.5 & 0 & 0 \\ 0 & 0 & 0 & 0 \\ 0 & 0 & 0 & 0 \end{bmatrix} \tag{37}$$

From DPM_A, it is clear that only the DISCO's in area 1 participate in Pool Co. transaction, others being inactive. The area participation factors are: $apf_{11} = 0.5$, $apf_{12} = 1 - apf_{11} = 0.5$, $apf_{21} = apf_{22} = 0.5$. The system is considered with AC interconnection only. Two cases are considered here for the investigation to determine the impact of additional source (DSTS) in the control areas namely

1 in presence of DSTS

2 in absence of DSTS plant in both areas.

PID and PI^{+}DD^{+} controller are engaged as secondary controller in areas one by one and the PID parameters are SFS optimised algorithm whose optimum values are tabulated in Table 2. Only two responses each for frequency deviation [Figures 4(a)–4(b)] and one for tie-power deviation [Figure 4(c)] are depicted in both cases to understand the system behaviour. From Figures 4(a)–4(c), it can be inferred that the peak deviations increases in absence of DSTS plant as it improves the generation profile of the system. The performance of both the parallel and proposed form is almost similar apart from the fact that, the overshoots and settling time in parallel form is more than in proposed PI^{+}DD^{+} controller. The oscillations in parallel form is observed to be slightly more than the proposed one. Thus, PI^{+}DD^{+} controller is considered to be better in terms of lesser overshoot, settling time and oscillations.

Now, the system under Pool Co. transaction is evaluated with various type of metaheuristic algorithms such as BBO (Rahman et al., 2016), QOHSA (Mahendra et al., 2017), FA (Debbarma et al., 2014) and SFS algorithm, widely used in AGC studies. This investigation needs to be carried out for evaluating the performance of the SFS (Iasef and Shuichi, 2016; Mellal and Zio, 2016; Saha and Saikia, 2017b; Sabir and Ibrir, 2019) algorithm. PI^{+}DD^{+} controller is employed in both control areas to lessen the area control error and hence, robust AGC. For a fair comparison, the population size in each algorithm is kept same and the tuned parameters of all the considered algorithms are shown in Table 3.

Figure 4 Comparison of frequency and tie-power responses during Pool Co. transaction (scenario 1), (a) ΔF_1 vs. time in absence of DSTS in both areas (b) ΔF_1 vs. time in presence of DSTS in both areas (c) ΔP_{tie12} vs. time in presence of DSTS in both areas (see online version for colours)

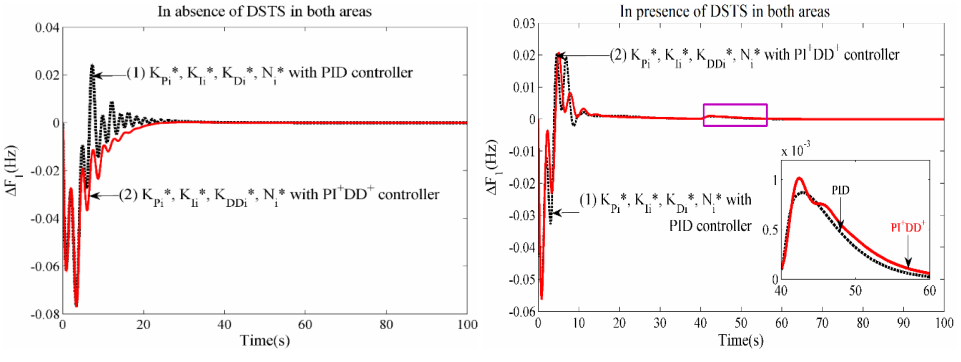

(a) (b)

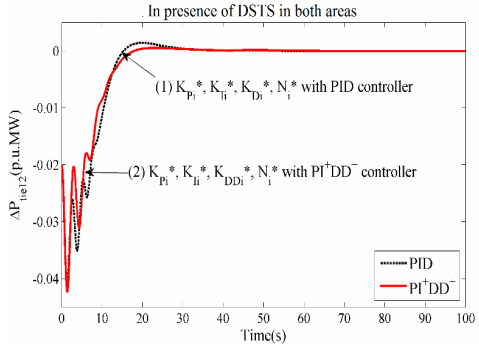

(c)

Table 2 Optimum classical PID and PI^+DD^+ controller parameters in areas 1 and 2 for Pool Co. transaction

Controller gains	*WoDSTS*		*wDSTS*	
	PID	*PI^+DD^+*	*PID*	*PI^+DD^+*
K^*_{P1}	0.459	0.614	0.454	0.753
K^*_{I1}	0.930	0.614	0.544	0.753
K^*_{D1}	0.402	-----	1.000	-----
K^*_{DD1}	-----	0.624	-----	0.814
N^*_1	54.77	96.92	29.4	37.9
K^*_{P2}	0.459	0.418	0.671	0.836
K^*_{I2}	0.930	0.566	0.866	0.977
K^*_{D2}	0.402	-----	-----	-----
K^*_{DD2}	-----	0.403	0.581	0.744
N^*_2	54.77	98.19	75.30	61.21

Table 3 Tuned parameters of various algorithms such as BBO, QOHSA, FA and FS

Sl. no.	*Algorithms*	*Parameters*
1	Biogeography-based optimisation	No. of habitats/population size = 50, generation limit, GL = 70, elites number, EN = 2, Mut probability, MP = 0.04 (4%), max. migration rates, MR = 1 and I = 1 (100%), SIVs per habitat number = SX1 + SX2, where, SX = number of optimised parameters in corresponding area of the system.
2	Quasi oppositional harmony search algorithm	Population size = 50, harmony memory search, HMS = consideration rate = 0.9, adjusting rate of pitch = 0.98, distance bandwidth = 0.0005, number of improvisations = 0.8, total number of search spaces = 40.
3	Firefly algorithm	Number of firefly = 50, maximum generation = 50, $\beta = 0.2$, $\alpha = 0.5$, $\gamma = 0.5$.

In each cases, the $PI^{+}DD^{+}$ controller parameters are optimised simultaneously (optimum controller parameters is not shown). The convergence characteristics in each case is plotted and compared and are depicted in Figure 5. The convergence characteristic using SFS algorithm is obtained from the previous case study under Pool Co. transaction in presence of DSTS plant in both areas.

Figure 5 Convergence characteristics of BBO, QOHSA, FA and SFS algorithm (see online version for colours)

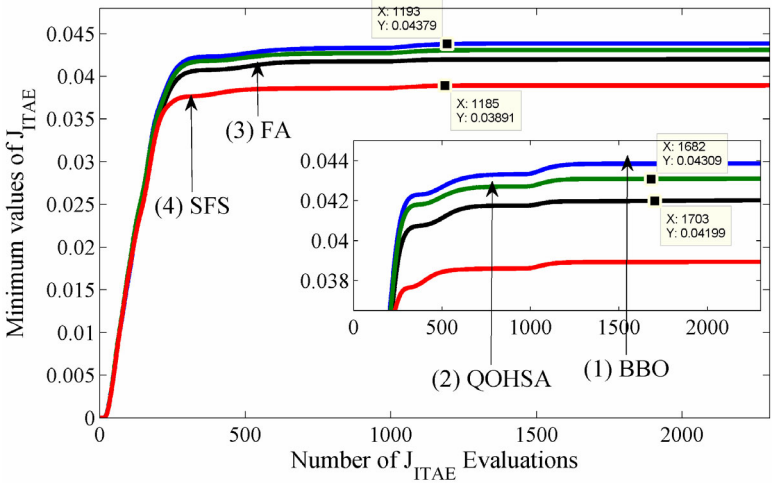

From Figure 5, it can be inferred that the performance of BBO, QOHSA and FA are almost the same whereas SFS algorithm outperforms others in terms of lesser J_{ITAE} values and slightly faster convergence than the other algorithms. Thus, SFS algorithm results into a better optimisation technique in terms of minimum value of convergence and faster convergence time with the system under Pool Co.-based transaction and $PI^{+}DD^{+}$ controller as secondary controller.

6.2 Scenario 2: bilateral transactions

In this case, the DISCOs can take independent decision to deal with any GENCO in its own control area or some other control areas. Here, the contracts relationships are framed according to DPM_B of equation (38). The demand for each DISCO is 0.02 p.u. ($\Delta P_L = 0.04$ p.u.).

$$DPM_{BT} = \begin{bmatrix} 0.3 & 0.4 & 0.2 & 0.2 \\ 0.2 & 0.2 & 0.2 & 0.4 \\ 0.3 & 0.1 & 0.3 & 0.3 \\ 0.2 & 0.3 & 0.4 & 0.1 \end{bmatrix} \tag{38}$$

6.2.1 Analysis of the two area gas-thermal system with various interconnections

The test system is facilitated with AC/DC links and AC/DC links with PLL dynamics and delay effects as described in Section 3 (Figure 2). A communication delay of 300 ms delay is considered for the second order PLL dynamics. The recommended range of time constant for DC line is 100–500 ms (Rakhshani et al., 2016). A time constant of 100 ms (T_{dc} = 0.1s) is considered here for investigation. Using equation (8), and considering K_{pi} = 2.24 Hz/p.u. and T_i = 0.l82 s, the control parameter gains of PLL function are considered: K_{f1} = 0.35, K_{f2} = 0.1, K_{f3} = 0.2, K_{AC} = 2, ζ_i = 0.32, ω_{ni} = 3.5. Considering each interconnection one at a time, SFS algorithm optimises the PI^+DD^+ controller parameters and the optimum values for AC/DC and AC/DC with PLL interconnections are tabulated in Table 4 in columns 2 to 4 respectively.

Table 4 Optimised parameters of PI^+DD^+ controller with various interconnections

PI^+DD^+	*AC only*	*AC/DC only*	*PLL (bilateral)*	*PLL (contract)*
K^*_{P1}	0.7758	0.8411	0.8948	0.8946
K^*_{I1}	0.5703	0.7109	0.7000	0.8886
K^*_{D1}	0.8618	0.7979	0.6908	0.4107
K^*_{DD1}	35.379	1.6720	0.0162	3.8286
N^*_1	0.8938	0.5225	0.5733	0.4837
K^*_{P2}	0.9990	0.9796	0.8322	0.3802
K^*_{I2}	0.5735	0.4487	0.3813	0.2260
K^*_{D2}	38.966	32.309	53.159	51.928
K^*_{DD2}				
N^*_2				

The comparison of system dynamic responses with different interconnections is presented in Figures 6(a)–6(c). Frequency deviation, tie – power and control signal deviation profile infer that DC link increases damping performance in terms of decreased peak deviation and lesser settling time. But with inclusion of PLL dynamics, system oscillation increases resulting into increased settling time and peak deviations. It is evident that the system

damping performance is affected by PLL and more efforts have to be provided to control oscillatory modes. Now, with AC/DC interconnection and PLL dynamics the generation profile for each source are evaluated and depicted in Figure 6(d).The apf's for GENCO1, GENCO2, GENCO3, and GENCO4 in presence of DSTS are 0.35, 0.65, 0.4, and 0.6. Considering DPM_B, the GENCOs in area 1 and area 2 will generate load power in the following manner: GENCO1 = 0.0081 p.u. MW, GENCO2 = 0.01481 p.u. MW, GENCO3 = 0.0091 p.u. MW and GENCO4 = 0.01398 p.u. MW respectively whereas a fixed generation from DSTS is considered to be 0.0169 p.u. MW [Figure 6(d)].

Figure 6 Comparison of frequency, tie power, control signal and power generation responses for various interconnections, (a) ΔF_2 vs. time (b) ΔP_{tie12} vs. time (c) control signal vs. time in area 1 (d) ΔP_g vs. time for each source in both areas 1 and 2 with PLL dynamics and delay effects (see online version for colours)

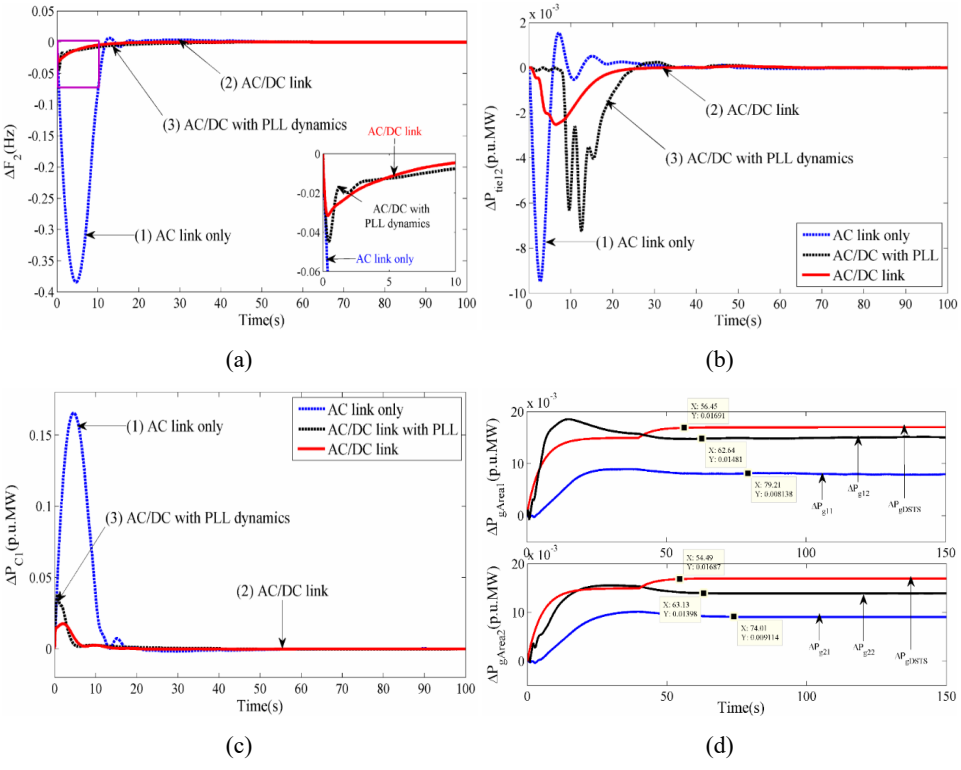

6.2.2 *Change in factors of PLL second order function on system dynamic responses*

Equation (8) states that changing the damping constant (ζ) and natural frequency (ω_{ni}) of PLL second order model, the system response may be affected. A comprehensive evaluation of PLL effect on system dynamic responses is carried out by changing one of the parameters between ω_n and ζ in PLL function maintaining the other parameter constant. In each case, the three control gains of SPMC are optimised along with other controller parameters. The brief explanation is covered in the following manner.

6.2.2.1 PLL effect upon change in ω_n with $\zeta = 1$

It is so considered that the PLLs in three areas with same ωn and ζ values as $\zeta_1 = \zeta_2 = \zeta_3 = \zeta_n$ and $\omega_1 = \omega_2 = \omega_3 = \omega_n$. $\omega_n = 0.1$, 1 and 2.5 are considered and comparison of system dynamic responses is done [Figures 7(a)–7(b)] with the nominal parameters of PLL considered in Subsection 6.2. The optimum PI^+DD^+ controller parameters in three control areas and the optimum control gains K_{f1}, K_{f2} and K_{AC} are noted in Tables 5 and 6.

Table 5 Optimised parameters of PI^+DD^+ controller with ω_n and ζ variation

	Variable ω_n and $\zeta = 1$			*Variable ζ and $\omega_n = 0.1$*		
	= 0.1	*= 1*	*= 2.5*	*= 0.3*	*= 0.5*	*= 0.8*
K^*_{P1}	0.907	0.553	0.564	0.751	0.778	0.729
K^*_{I1}	0.698	0.743	0.736	0.715	0.639	0.637
K^*_{DD1}	0.760	0.337	0.264	0.317	0.305	0.174
N^*_1	31.89	50.92	45.94	40.84	33.28	32.35
K^*_{P2}	0.846	0.538	0.483	0.751	0.560	0.576
K^*_{I2}	0.981	0.878	0.813	0.715	0.805	0.814
K^*_{DD2}	0.545	0.434	0.370	0.317	0.595	0.429
N^*_2	63.50	39.43	31.80	40.84	40.02	32.49

Figure 7 Comparison of frequency, control signal and tie power responses under ω_n variation, (a) ΔF_1 vs. time (b) control signal vs. time in area 1 (c) control signal vs. time in area 2 (d) ΔP_{tie12} vs. time (see online version for colours)

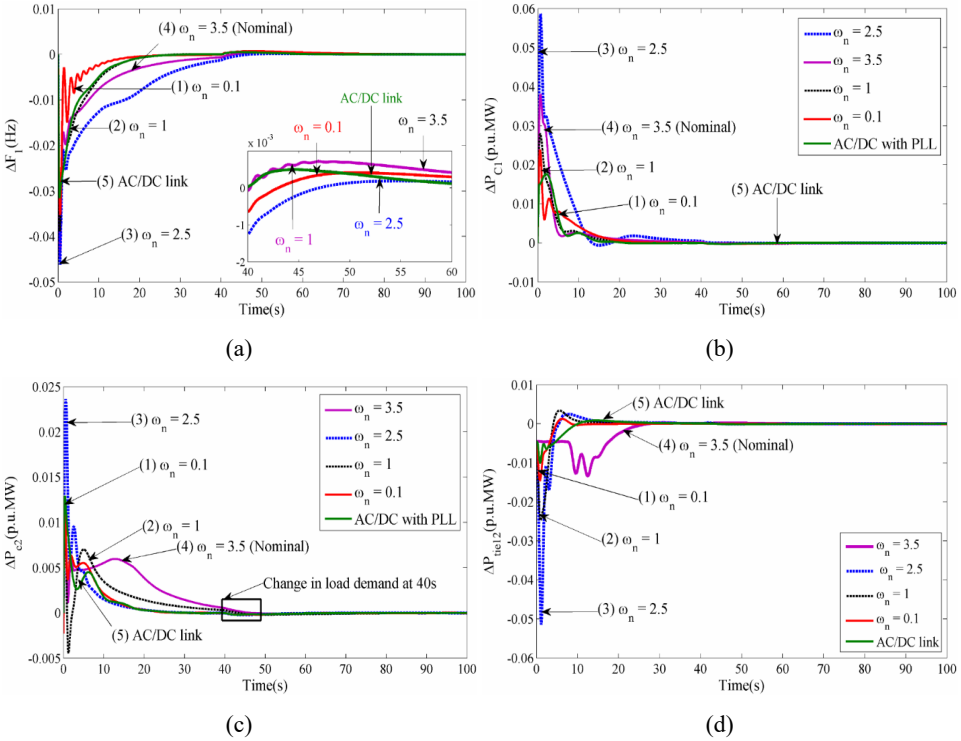

It is evident that lower values ω_n of provides lesser overshoot, undershoot and settling time than others. However, variation of may provide some more information of selection of PLL gains. Thus, the same is taken into account in the next study.

6.2.2.2 PLL effect upon change in ζ_1 with $\omega_n = 2.5$

In Subsection 6.2.2.1, it is seen that with PI^+DD^+ as secondary controller, the system responses with $\omega_n = 0.1$ and $\zeta = 1$ in PLL function are improved than other considered values. So, to make the analysis extensive, Subsection 6.2.2.2 is represented with a change in $\zeta_1 = \zeta_2 = \zeta_3 = \zeta_n$ and with $\omega_n = 0.1$. Three values of ζ (0.3, 0.5 and 0.8) are considered with nominal parameters of PLL (Subsection 6.2). The optimum PI^+DD^+ controller parameters and SPMC control gains with corresponding changes in ζ are noted in Tables 5 and 6 respectively. The system responses comparison is depicted in Figures 8(a)–8(d).

Table 6 Optimised parameters of controller when ω_n and ζ are changed keeping one fixed

Variable ω_n, fixed $\zeta = 1$			*Variable ζ, fixed $\omega_n = 1$*		
$\omega_n = 0.1$	K_{f1}	0.6812	$\zeta = 0.3$	K_{f1}	0.6333
	K_{f2}	0.5195		K_{f2}	0.3564
	K_{ac}	3.6387		K_{ac}	3.6616
$\omega_n = 1$	K_{f1}	0.5309	$\zeta = 0.5$	K_{f1}	0.7244
	K_{f2}	0.1460		K_{f2}	0.4423
	K_{ac}	2.7105		K_{ac}	3.3185
$\omega_n = 2.5$	K_{f1}	0.5291	$\zeta = 0.8$	K_{f1}	0.7533
	K_{f2}	0.2602		K_{f2}	0.4643
	K_{ac}	3.0168		K_{ac}	3.2369

It is observed that, at lower values of ζ, system is more oscillatory and increase in the same reduces the oscillations and thereby decreases the peak overshoot, peak undershoot and settling time. Thus, the optimum set of PLL control gains are $\zeta = 0.8$ and $\omega_n = 0.1$. Also, considering unity damping will surely improve the dynamic responses.

6.3 Scenario 3: violation of scheduled contract

When DISCO's demand more power than agreed, i.e., violating the contract, it is termed as contract violation. The excess power demanded will have to be mitigated by the GENCO's in the area. Let us assume that DISCO1 demands an excess load of 0.01 p.u. MW from nominal 0.04 p.u. MW. Thus, area 1 can be totalled by the summation of local load of DISCO1, DISCO2 and contract violation. Considering DPM_B in case 2 [by equation (38)].

$$\Delta P_L = 0.02 + 0.02 + 0.01 = 0.05 \text{ p.u. MW}.$$

The apf's 0.5, 0.5, 0.5 and 0.5 are based on production schedule of concerned DPM_B given by equation (38). Also, the violation in load demand may not be static. It may be changing in due course of time when considered in realistic scenario. Thus, this study is extended to violation of demand by 2%, 3% and 6%, resulting which the local load

becomes 0.06 (= 0.04 + 0.02) p.u., 0.07 (= 0.04 + 0.03) p.u. and 0.10 (= 0.04 + 0.06) p.u. respectively. SFS algorithm is utilised to optimise the controller parameters for each violation and the optimum parameters are noted in Table 7. It is of utmost concern that how the system behaves for higher violations and at the same time, the best set of PLL second order function should stand well during the changed situations. The comparison of dynamic responses for the aforementioned cases are presented in Figures 9(a)–9(d).

Figure 8 Comparison of frequency, control signal and tie power responses under ζ variation, (a) ΔF_1 vs. time (b) control signal vs. time in area 1 (c) control signal vs. time in area 2 (d) ΔP_{tie12} vs. time (see online version for colours)

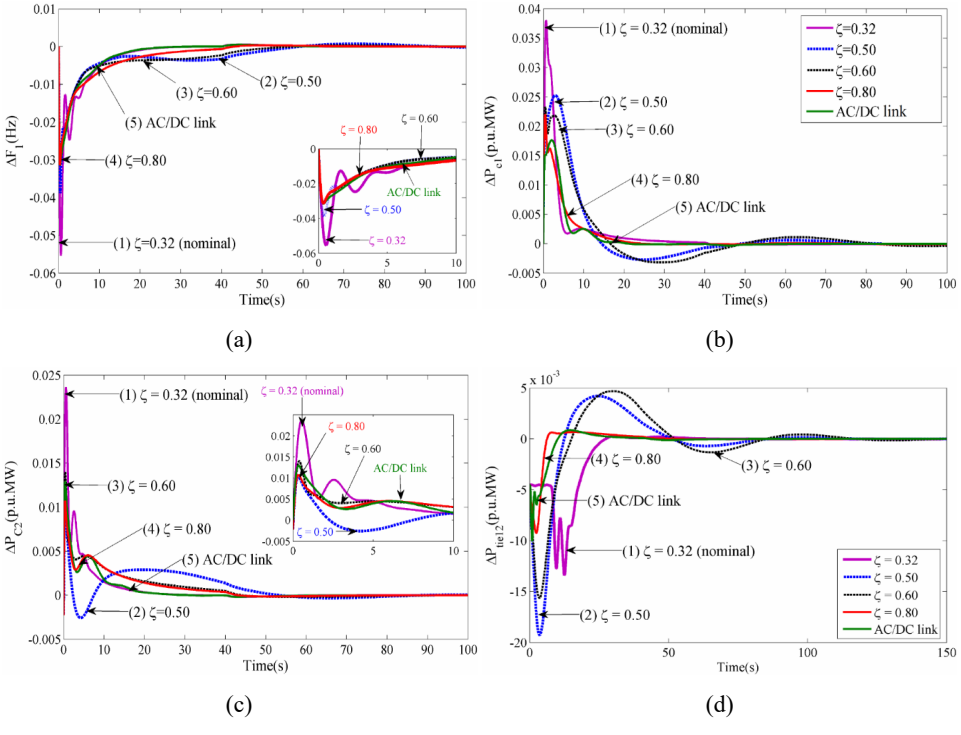

Table 7 Optimum controller parameters of PI⁺DD⁺ for contract violation of 1%, 2%, 3% and 10% respectively

	Contract violation of			
	+1%	*+2%*	*+3%*	*+10%*
K^*_{P1}	0.8155	0.7419	0.9215	0.8946
K^*_{I1}	0.7171	0.7804	0.7674	0.8886
K^*_{DD1}	0.2400	0.1194	0.5809	0.4107
N^*_1	49.767	43.973	0.0004	3.8286
K^*_{P2}	0.6169	0.6153	0.6048	0.4837
K^*_{I2}	0.8939	0.8348	0.6039	0.3802
K^*_{DD2}	0.7409	0.6209	0.2263	0.2260
N^*_2	41.420	35.436	46.859	51.928

Figure 9 Comparison of frequency, tie-power and power generation responses for 1%, 2%, 3% and 6% contract violation respectively from 4% nominal (bilateral transaction), (a) ΔF_1 vs. time (b) ΔP_{tie12} vs. time (c) ΔP_{g1} vs. time (d) ΔP_{g2} vs. time for 6% violation of load demand (see online version for colours)

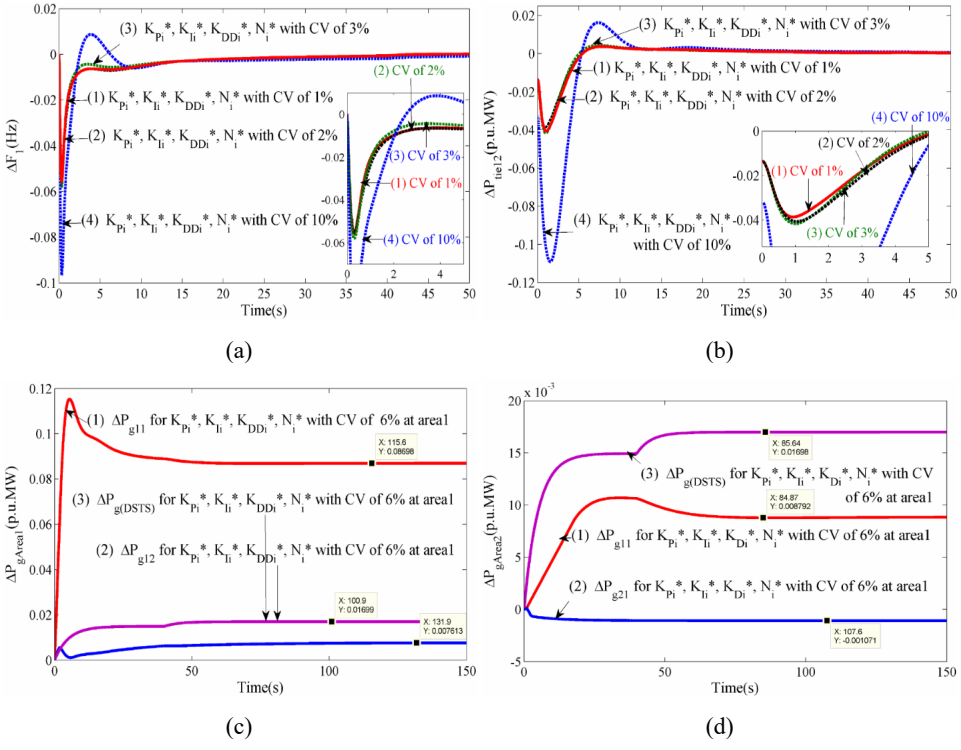

Dynamic responses [Figures 9(a)–9(b)] clearly states that the undershoot increases with increase in contract violation, however, the time to reach the steady state remains almost the same. The overshoot in all the changed condition is within safe limits. Also, the generation profile matches the demand.

6.4 Scenario 4: performance of PI⁺DD⁺ controller along with best suited PLL parameters against change in thermal and gas plant system parameters

It is evident that change in time constants of gas and thermal plant may provide frequency and tie-power excursion (Bevrani and Hiyama, 2014; Kumar and Kothari, 2005). It is necessary to design the test system accordingly so that the optimum controller parameters along with second order PLL function can stand well during times of change. Thus, the deciding factors of performance of thermal and gas plant such as governor, turbine, fuel and compressor discharge time constant are varied for ±50% and the system behaviour is observed for the change. The optimum controller parameters at changed scenario are tabulated in Table 8. The optimum PI^+DD^+ controller parameters from bilateral transaction (scenario 2) are considered as nominal controller parameters. Using these optimum values, the dynamic responses for change in T_{gi} (±50% of 0.08 s), T_t (±50% of 0.3 s), T_f (±50% of 0.239 s) and T_{cd} (±50% of 0.2 s) against nominal values are obtained and compared in Figures 10(a)–10(c). From Figures 10(a)–10(c), it is evident

that very fewer changes are observed due to ±50% change in T_{gi}, T_{ti}, T_{fi} and T_{cdi}. Thus, it can be inferred that the optimum controller parameters along with optimum PLL gains and other parameters need not be changed during ±50% change in time constants of thermal and gas turbine time-constants and hence robustness is ensured.

Table 8 Optimum $PI^{+}DD^{+}$ controller parameters at ±50% change in T_{gi}, T_{ti}, T_{fi} and T_{cd}

	+50% of nominal values of				*–50% of nominal values of*			
	T_{cd}	T_f	T_g	T_t	T_{cd}	T_f	T_g	T_t
K^*_{P1}	0.9797	0.8526	0.9730	0.9527	0.9038	0.9012	0.9134	0.9257
K^*_{I1}	0.6097	0.6959	0.6356	0.6318	0.6648	0.6776	0.6427	0.6614
K^*_{DD1}	0.8324	0.8090	0.8171	0.8441	0.7632	0.7909	0.8690	0.8397
N^*_1	2.3347	21.702	1.6168	1.1097	30.998	39.880	1.9612	2.3110
K^*_{P2}	0.6515	0.8320	0.6704	0.6387	0.8515	0.8771	0.6154	0.6408
K^*_{I2}	0.9090	0.9697	0.8829	0.9106	0.9965	0.9904	0.9355	0.9439
K^*_{DD2}	0.4591	0.4665	0.4592	0.4375	0.5727	0.5572	0.4818	0.4306
N^*_2	51.693	58.555	51.665	56.418	56.860	53.289	56.857	56.765

Figure 10 Comparison of frequency and tie-power responses for ±50% change in time constants of thermal and gas turbine time-constants such as T_{gi}, T_{ti}, T_{fi} and T_{cdi}, (a) ΔF_1 vs. time for ± 50% change in T_{fi} and T_{cdi} (b) ΔP_{tie12} for ±50% change in T_{gi} and T_{ti} (see online version for colours)

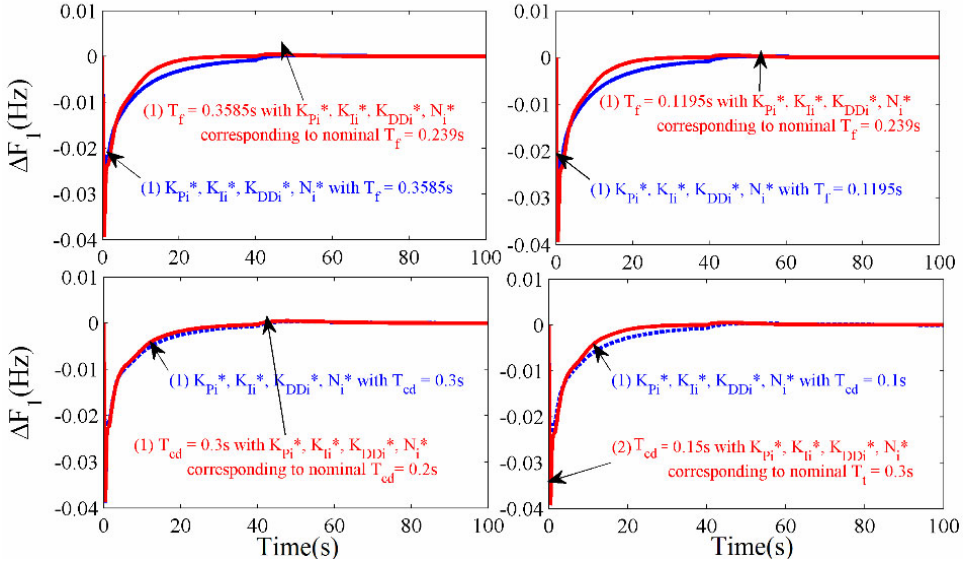

(a)

Figure 10 Comparison of frequency and tie-power responses for ±50% change in time constants of thermal and gas turbine time-constants such as T_{gi}, T_{ti}, T_{fi} and T_{cdi}, (a) ΔF_1 vs. time for ± 50% change in T_{fi} and T_{cdi} (b) ΔP_{tie12} for ±50% change in T_{gi} and T_{ti} (continued) (see online version for colours)

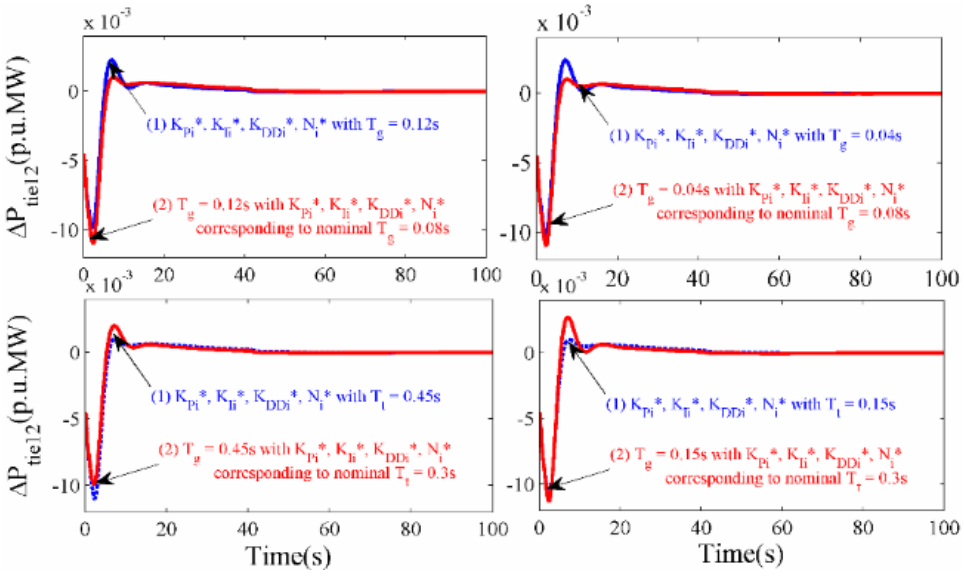

(b)

7 Conclusions

The effects of second order PLL in an AC/DC interconnection is evaluated for a two-area multi-machine gas-thermal system in presence of nonlinearity such as GRC, GDB and time-delay. Enhanced use of HVDC interconnection in open marker scenario urge to analyse the proper modelling of HVDC with PLL function in multi-machine system. Following are the contributions:

a Eigenvalue analysis of the test system with various interconnection namely AC, AC/DC link, AC/DC with PLL effects confirms the stability of the system. Test system with AC/DC interconnection is observed to be more stable than others. However, analysing the same with optimum PLL gains and parameters tend the system with AC/DC and PLL effects more stable.

b The proposed $PI^{+}DD^{+}$ controller when employed as secondary controller in the multi-area gas-thermal system under Pool Co. transaction outperforms parallel PID form in terms of overshoot and settling time whereas the undershoot remains almost the same.

c The proposed system with various interconnections under bilateral transactions infers that AC/DC system damps out the oscillations to a superior extent than AC/DC with PLL dynamics lags and AC interconnection. Proper tuning of parameters of PLL second order function brings the performance of presence of PLL similar to AC/DC

interconnection. Any type of system can be made to perform like AC/DC on proper tuning of PLL parameters.

d During contract violation case, the performance of system is expected to deviate. But upon violation of contracts by the DISCO in area 1 by 1%, 2%, 3% and 6% from nominal 4% (scenario 2 bilateral transaction), the proposed $PI^{+}DD^{+}$ along with best suited parameters commensurate with nominal responses under bilateral transactions, although very less changes are observed which falls under safe limits.

e The controller performs well during changed conditions of gas and thermal plant time constants. Although, –50% changes in time constants try to deviate the performance from nominal but the system retains its steady state within a fixed interval of time. Thus, robustness of the optimum parameters of $PI^{+}DD^{+}$ controller is ensured for ±50% change in T_{gi}, T_{ti}, T_{fi} and T_{cd}.

References

Arya, Y. (2017) 'AGC performance enrichment of multi-source hydrothermal gas power systems using new optimized FOFPID controller and Redox flow batteries', *Energy*, Vol. 127, pp.704–715, https://doi.org/10.1016/j.energy.2017.03.129.

Arya, Y. and Kumar, N. (2016) 'AGC of a multi-area multi-source hydrothermal power system interconnected via AC/DC parallel links under deregulated environment', *International J. of Electrical Power & Energy Systems*, Vol. 75, pp.127–138, http.s://doi.org/10.1016/j.ijepes. 2015.08.015.

Arya, Y. and Kumar, N. (2017) 'BFOA-scaled fractional order fuzzy PID controller applied to AGC of multi-area multi-source electric power generating systems', *Swarm and Evolutionary Computation*, Vol. 32, pp.202–218, https://doi.org/10.1016/j.swevo.2016.08.002.

Bevrani, H. and Hiyama, T. (2014) *Intelligent Automatic Generation Control*, 2nd ed., CRC Press, Boca Raton, https://doi.org/10.1201/b10869.

Bjorn, H.B. and Ove, S.G. (1998) 'Automatic generation control in a deregulated power system', *IEEE Trans. on Power Systems*, Vol. 13, No. 4, pp.1401–1406.

Das, D.C., Sinha, N. and Roy, A.K. (2014) 'Small signal stability analysis of dish-Stirling solar thermal based autonomous hybrid energy system', *International Journal of Electrical Power & Energy Systems*, Vol. 63, pp.485–498, https://doi.org/10.1016/j.ijepes.2014.06.006.

Debbarma, S., Saikia, L.C. and Sinha, N. (2014) 'Solution to automatic generation control problem using firefly algorithm optimized $I_{\lambda}D_{\mu}$ controller', *ISA Transactions*, Vol. 53, No. 2, pp.358–366.

Donde, V., Pai, M.A. and Ian, A.H. (2001) 'Simulation and optimization in an AGC system after deregulation', *IEEE Trans. on Power Systems*, Vol. 16I, No. 3, pp.481–489.

Elgerd, O.I. and Fosha, C.E. (1970) 'Optimum megawatt frequency control of multi-area electric energy systems', *IEEE Trans Power Apparatus Syst.*, Vol. 89, No. 4, pp.556–563.

Guha, D., Roy, P.K. and Banerjee, S. (2017) 'Study of differential search algorithm based automatic generation control of an interconnected thermal-thermal system with governor dead-band', *Applied Soft Computing*, Vol. 52, pp.160–175, https://doi.org/10.1016/j.asoc. 2016.12.012.

Hamid, S. (2015) 'Stochastic fractal search: a powerful metaheuristic algorithm', *Knowledge-Based Systems*, Vol. 75, pp.1–18, https://doi.org/10.1016/j.knosys.2014.07.025.

Hota, P.K. and Banaja, M. (2016) 'Automatic generation control of multi-source power generation under deregulated environment', *International Journal of Electrical Power & Energy Systems*, Vol. 75, pp.205–214, https://doi.org/10.1016/j.ijepes.2015.09.003.

Iasef, M.R. and Shuichi, A. (2016) 'Computational design of a nature-inspired architectural structure using the concepts of self-similar and random fractals', *Automation in Construction*, Vol. 66, pp.53–58, https://doi.org/10.1016/j.autcon.2016.03.010.

Ibraheem, N. and Bhatti, T.S. (2014) 'AGC of two area power system interconnected by AC/DC links with diverse sources in each area', *International Journal of Electrical Power & Energy Systems*, Vol. 55, pp.297–304, https://doi.org/10.1016/j.ijepes.2013.09.017.

Johnson, M.A. and Moradi, M.H. (2000) *PID Control: New Identification and Design Methods*, Springer-Verlag, Limited, London.

Kumar, P.I. and Kothari, D.P. (2005) 'Recent philosophies of automatic generation control strategies in power systems', *IEEE Trans. Power Syst.*, Vol. 20, No. 1, pp.346–357.

Kundur, P. (1994) *Power System Stability and Control*, McGraw-Hill, New York.

Lasantha, M. (2014) 'Characterisation of gas turbine dynamics during frequency excursions in power networks', *IET Generation, Transmission & Distribution*, Vol. 8, No. 10, pp.1733–1743.

Mahendra, N., Shiva, C.K. and Mukherjee, V. (2017) 'TCSC based automatic generation control of deregulated power system using quasi-oppositional harmony search algorithm', *Engineering Science and Technology*, Vol. 20, No. 4, pp.1380–1395.

Mellal, M.A. and Zio, E. (2016) 'A penalty guided stochastic fractal search approach for system reliability optimization', *Reliability Engineering & System Safety*, Vol. 152, pp.213–227, https://doi.org/10.1016/j.ress.2016.03.019.

Miroslav, R. et al. (2014) 'Series PID controller tuning based on the SIMC rule and signal filtering', *Journal of Process Control*, Vol. 24, pp.687–693, https://doi.org/10.1016/j.jprocont.2013.10.001.

Rahman, A., Saikia, L.C. and Sinha, N. (2016) 'AGC of dish-Stirling solar thermal integrated thermal system with biogeography based optimised three degree of freedom PID controller', *IET Renewable Power Generation*, Vol. 10, No. 8, pp.1161–1170.

Rahman, A., Saikia, L.C. and Sinha, N. (2017) 'Automatic generation control of an interconnected two-area hybrid thermal system considering dish-Stirling solar thermal and wind turbine system', *Renewable Energy*, Vol. 105, pp.41–54.

Rakhshani, E. et al. (2012) 'Effect of VSC-HVDC on load frequency control in multi-area power system', *Energy Conversion Congress and Exposition (ECCE)*, IEEE, Raleigh, NC, USA, 15–20 September.

Rakhshani, E. et al. (2014) 'Integration of renewable generation for frequency support of HVDC/AC interconnected systems under power market scenario', *PES General Meeting| Conference & Exposition*, IEEE, National Harbor, MD, USA, 27–31 July.

Rakhshani, E. et al. (2016) 'Effects of PLL and frequency measurements on LFC problem in multi-area HVDC interconnected systems', *International J. of Electrical Power & Energy Systems*, Vol. 81, pp.140–152.

Rao, C.S., Siva, N.S. and Raju, P.S. (2009) 'Automatic generation control of TCPS based hydrothermal system under open market scenario: a fuzzy logic approach', *International J. of Elect. Power & Energy Systems*, Vol. 31, Nos. 7–8, pp.315–322.

Rao, G.S. and Das, D. (2015) 'Real power and frequency control of a small isolated power system', *Electrical Power and Energy Systems*, Vol. 64, pp.221–232.

Sabir, A. and Ibrir, S. (2019) 'A robust control scheme for grid-connected photovoltaic converters with low-voltage ride-through ability without phase-locked loop', *ISA Transactions* [online] https://doi.org/10.1016/j.isatra.2019.05.027.

Saha, D. and Saikia, L.C. (2017a) 'Impact of phase-locked loop on system dynamics of a CCGT incorporated diverse source system employed with AC/DC interconnection', *Journal of Renewable and Sustainable Energy*, Vol. 9, No. 45506, pp.1–24.

Saha, D. and Saikia, L.C. (2017b) 'Automatic generation control of a multi-area CCGT-thermal power system using stochastic search optimised integral minus proportional derivative controller under restructured environment', *IET Generation, Transmission & Distribution*, Vol. 11, No. 15, pp.3801–3813, https://doi.org/10.1016/j.renene.2016.12.048.

Sharma, G., Ibraheem, N., Niazi, K.R. and Bansal, R.C. (2016) 'Optimal AGC of a multi-area power system with parallel AC/DC tie lines using output vector feedback control strategy', *International J. of Electrical Power & Energy Systems*, Vol. 81, pp.22–31, https://doi.org/10.1016/j.ijepes.2016.02.007.

Singh, P.K.P., Majhi, S. and Kothari, D.P. (2014) 'LFC of an interconnected power system with multi-source power generation in deregulated power environment', *International Journal of Electrical Power & Energy Systems*, Vol. 57, pp.277–286, https://doi.org/10.1016/j.ijepes.2013.11.058.

Wang, Y., Chen, X., Wang, Y. and Gong, C. (2019) 'Analysis of frequency characteristics of phase-locked loops and effects on stability of three-phase grid-connected inverter', *Electrical Power and Energy Systems*, Vol. 113, pp.652–663, https://doi.org/10.1016/j.ijepes.2019.06.016.

Zhou, J.Z. et al. (2014) 'Impact of short-circuit ratio and phase-locked-loop parameters on the small-signal behaviour of a VSC-HVDC converter', *IEEE Transactions on Power Delivery*, Vol. 29, No. 5, pp.2287–2296.

Appendix 1

System parameters considered

Governor time constant, T_{gi} = 0.08s

Turbine time constant, T_{ti} = 0.3s

Reheat time constant, T_{ri} = 10s

Reheat turbine gain, K_{ri} = 5

Power system time constant, K_{ps} = 120

Power system time constant, T_{ps} = 20s

Compressor discharge time constant, T_{cdi} = 0.2s

Fuel valve time constant, T_{fi} = 0.23s

Combustion chamber time constant, T_{cri} = 0.3s

Gas turbine speed governor lead time constant, X_i = 0.6

Gas turbine speed governor lag time constant, Y_i = 1s

Gas turbine gain of valve position, b_i = 0.05

Gas turbine time constant of valve position, c_i = 1

Power system gain, Inertia, H_i = 5s

Tie-power synchronizing coefficient, T_{ij} = 0.0083 p.u.MW

Speed regulation parameter, R_i = 2.4 Hz/p.u.MW

Frequency, F = 60 Hz.

Appendix 2

Nomenclature for considered state variables

ΔF_i Frequency deviation of i^{th} area

ΔP_{gij} Deviation in j^{th} generating source of i^{th} area

ΔP_{Ti} Deviation in intermediate step in reheat turbine of thermal plant of i^{th} area

ΔP_{g0i} Deviation in steam turbine governor output of thermal plant of i^{th} area

ΔP_{cri} Deviation in intermediate state of fuel system combustor of gas turbine of i^{th} area

ΔP_{CPi} Deviation in intermediate state of fuel system and combustor of gas turbine of i^{th} area

ΔP_{gTi} Deviation in valve positioned of gas turbine of i^{th} area.